Hydrogen-rich gas production by steam reforming of *n*-dodecane. Part II: Stability, regenerability and sulfur poisoning of low loading Rh-based catalyst

A. Vita*, C. Italiano, L. Pino, M. Laganà, V. Recupero

CNR-ITAE "Nicola Giordano", Via Salita S. Lucia sopra Contesse 5, 98126, Messina, Italy

ABSTRACT

In this paper, 0.6 wt.% Rh/CeO_2 catalyst was synthesized by the Solution Combustion Synthesis (SCS) method, producing a low-cost noble metal-based system due to the simultaneous high dispersion and low metal phase content. The catalyst was characterized by the XRD, N_2-physisorption, CO-chemisorption, TPR, TPO and TEM measurements. Deactivation by carbon deposition was investigated in Steam Reforming (SR) of *n*-dodecane, used as surrogate for diesel fuel, in order to explore the appropriate coke-free reaction conditions. The catalyst regenerability was also investigated. Then, the effect of sulfur poisoning was studied in SR of *n*-dodecane doped with thiophene, used as model compound for the organic sulfur in diesel fuel. Stability tests were performed at various steam-to-carbon ratio (S/C = 1–2.5), space velocity (GHSV = 16,000–40,000 h^{-1}) and sulfur content (0–100 ppm S). In order to avoid carbon/coke deposition due to cracking of *n*-dodecane, tests were carried out using the temperature-controlled bed configuration (500–800 °C) previously studied.

Stable catalytic performance was achieved under sulfur-free condition. Constant H_2 concentration (62%, N_2-free basis) in the product mixture and absence of carbon deposition were observed at S/C = 1.5 for 100 h of time-on-stream. Catalyst deactivation was observed in the presence of sulfur, mainly due to graphitic carbon deposition. Higher amount of steam allowed improving the carbon gasification and the sulfur tolerance, enhancing the catalytic stability of the Rh/CeO_2 system.

© 2017 Elsevier B.V. All rights reserved.

1. Introduction

In the transition towards a sustainable and environmental friendly energy system, the production of hydrogen from liquid hydrocarbons could help to overcome the lack of production and distribution infrastructure of hydrogen [1,2]. Particularly, liquid fuels, derived from either fossil or renewable sources, represent an attractive source of hydrogen for both on-site and on-board fuel cell systems, since they are easily transportable and their distribution infrastructures are readily available [3,4]. Furthermore, gasoline, diesel and jet fuels are prospective candidates for fuel cell hydrogen, because they provide high energy density compared to the other fuels [5,6]. However, they also contain coke precursors as well as sulfur compounds such as thiophenes, benzothiophenes and dibenzothiophenes [7].

Several conventional technologies are available to produce hydrogen, among which steam reforming (SR) remains one of the most economical alternatives due to the high hydrogen yield in the effluent gas [8,9]. The fuel reforming reaction is expressed by the following equation:

$$C_mH_n + mH_2O \rightarrow mCO + (m + 1/2n)H_2, \Delta H > 0$$
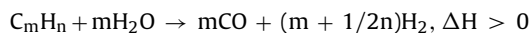
Much recent work has focused on the development of cheap, active, poison resistant and renewable catalysts. Typically, SR catalysts deactivate within a few hours of on-stream exposure, mainly due to coking and sulfur poisoning [1,10]. Moreover, steam reforming is usually carried out at high temperature which can lead to loss in surface area due to sintering [5,11]. Noble metal-based catalysts (Pt, Ru, Rh) have better activity and stability of conventional catalysts at higher temperature and can be used for steam reforming of long-chain hydrocarbons [12]. In a previous work [13], we studied the SR of sulfur-free *n*-dodecane over a Pt/CeO_2 catalyst, prepared by solution combustion synthesis. The synthesized system showed a catalytic activity comparable with that of the commercial Rh/ZDC (Rh/Zirconia-doped-Ceria). Coke

* Corresponding author.
E-mail addresses: antonio.vita@itae.cnr.it, vitaantonio72@gmail.com (A. Vita).

deposition due to cracking phenomena has been avoided using an optimized temperature-controlled bed configuration with temperature ranging between 500 and 800 °C, while the physico-chemical and morphological properties of the Pt/CeO$_2$ system further limited carbon deposition mainly related to Boudouard and reverse gasification reaction. The adopted synthesis method allowed inducing a strong metal-support interaction (SMSI) strictly connected with the observed high catalytic activity and stability during n-dodecane steam reforming. Thus, high and stable H$_2$ production (ca. 73%, dry and N$_2$-free basis) was observed under start-up and shut-down cycles for 50 h at S/C = 2.5 and GHSV = 16000 h^{-1} [13].

Although this system is extremely efficient for sulfur-free n-dodecane SR, questions remain about the deactivation associated with the presence of sulfur in the liquid fuels. Xie and co-workers [14] compared the influence of the type of metal on the sulfur tolerance and carbon resistance of supported noble metal catalysts in SR of liquid hydrocarbons. The sulfur presence deactivated all the Al$_2$O$_3$-supported noble metal catalysts with the following order: Rh < Pt ≤ Pd ≤ Ru. The strong sulfur tolerance of Rh/Al$_2$O$_3$ was related to the strong resistance of Rh to the sulfur-induced withdrawal compared to the other metals. Moreover, previous studies demonstrated that sulfur is adsorbed on the same sites as those involved in carbon formation. Thus, because of the better sulfur tolerance, Rh catalysts showed also a much lower carbon deposition rate [15]. Additionally, particular attention is currently focused on the role of the support. Ceria loaded with metals (e.g. Pt, Rh, Pd) was found to be promising support to process liquid hydrocarbons due to the high oxygen ion conductivity and oxygen storage capacity of ceria [16].

Unfortunately, the application of noble metal-based catalysts is greatly limited due to the high cost and low abundance. However, the synthesis of highly dispersed system allows the decrease of the metal phase loading and the simultaneously increase of its catalytic activity [17,18]. As reported by Xing et al. [19], this could be a sensible way to use high active/stable and reduced-cost noble metal-based catalysts.

In this study, a 0.6 wt.% Rh/CeO$_2$ catalyst was synthesized by the solution combustion synthesis and characterized by the BET (Brunauer-Emmett-Teller) method, X-ray diffraction (XRD), CO-chemisorption and H$_2$ temperature-programmed reduction (H$_2$-TPR). The catalytic tests were carried out using the experimental set-up previously described [13] in order to avoid carbon/coke deposition due to cracking of n-dodecane. The performance of Rh/CeO$_2$ catalyst was studied towards SR of sulfur-free n-dodecane, used as surrogate for diesel fuel, in order to explore the appropriate coke-free reaction conditions. Stability tests were carried out over 100 h of time-on-stream at GHSV = 16,000 h^{-1}, varying the steam-to-carbon (S/C) molar ratio from 2.5 to 1.0. Moreover, the regeneration ability of the system was studied at S/C = 1 and GHSV = 40,000 h^{-1} through deactivation/regeneration cycles.

Then, the sulfur tolerance (30, 60 and 100 ppm of sulfur) was investigated under SR of n-dodecane doped with thiophene, used as model compound for the organic sulfur in diesel fuel. In addition to characterization of the fresh catalysts, transmission electron microscopy (TEM) and temperature programmed oxidation (TPO) were employed to characterize the metal particle size and to identify the carbon species in the used catalysts after reforming reaction.

2. Experimental section

2.1. Catalysts synthesis

Rh/CeO$_2$ catalyst and CeO$_2$ support were synthesized by the Solution Combustion Synthesis (SCS) method previously described [20]. The precious Rh loading was set to 0.6 wt.% and confirmed by chemical analysis (ICP/OES). High-purity reagent-grade were used as received: rhodium nitrate (Rh(NO$_3$)$_3$, Aldrich) and ammonium cerium nitrate ((NH$_4$)$_2$Ce(NO$_3$)$_6$, Alfa Aesar) as metal precursors, while urea (CH$_4$N$_2$O, Alfa Aesar) as fuel. Stoichiometric amounts of metal salts and urea were dissolved in the minimum quantity of distilled water. The obtained solution was aged in a glass beaker of 600 cm^3 and introduced into a furnace preheated at 350 °C. After several minutes, the combustion occurred with rapid increase in temperature and gas evolution (N$_2$, CO$_2$, H$_2$O), due to the reaction between metal precursors and fuel. The resulting spongy powder was naturally cooled down to room temperature in few minutes. The temperature profiles (not shown) were registered using a thermocouple placed within the starting solution; an abrupt rise in temperature from 100 °C (water boiling point) to the flame temperature (maximum value), equal to 866 and 494 °C for Rh/CeO$_2$ and CeO$_2$ samples respectively, was recorded. Although an error in the temperature reading can not be excluded, that difference is mainly due to the different amounts of precursors and fuel, responsible for the heat released during the combustion. The synthesized systems were calcined at 600 °C for 2 h (heating rate set at 5 °C min^{-1}). Before catalytic test, Rh/CeO$_2$ catalyst (200–600 μm) was diluted with quartz particles (catalyst:quartz = 1:1) to ensure an optimal temperature distribution through the catalytic bed, followed by reduction in situ with 50% H$_2$/N$_2$ stream (30 Nml·min^{-1}) at 300 °C for 1 h.

2.2. Catalysts characterization

Specific surface area was estimated from adsorption/desorption isotherms at liquid nitrogen temperature (−196 °C) on *Micromeritics ASAP 2020* instrument. The isotherms were elaborated according to the Brunauer-Emmet-Teller (BET) equation. The samples were degassed by heating at 300 °C under vacuum before the BET analysis.

X-ray powder diffraction (XRD) patterns were recorded by a *Philips X-Pert 3710* diffractometer at a scanning speed of 1.50° min^{-1} over the range 2θ = 20°–75°. The diffractometer was equipped with a Cu Kα radiation source, operating at 40 kV and 20 mA. The peaks were assigned according to the PCPFWIN database. The CeO$_2$ crystallite size was calculated using the Scherrer equation based on the CeO$_2$ (111) reflection peak.

CO-chemisorption measurement was carried out on a *Micromeritics ChemiSorb 2750* instrument equipped with a thermal conductivity (TCD) detector. Following the method proposed by Takeguchi et al. [21], the catalytic sample was: i) reduced under H$_2$ flow (30 Nml·min^{-1}) at 200 °C for 30 min; ii) oxidized under pure O$_2$ flow (30 Nml min^{-1}) at room temperature for 10 min; iii) treated under CO$_2$ flow (30 Nml min^{-1}) at room temperature for 10 min; iv) reduced under pure H$_2$ flow (30 Nml min^{-1}) at room temperature for 30 min. Then, a mixture of 10% CO in He was injected in pulses of 600 NμL each, until the fulfilment of constant outlet peaks. This method prevents the CO adsorption on CeO$_2$ as carbonate species [21]. The rhodium dispersion (D$_{Rh}$) was calculated from the amount of chemisorbed CO, through the equation $D_{Rh} = f_{CO/Rh} \cdot V_{CO}/22414 \cdot M_{Rh}/L_{Rh}$, where f$_{CO/Rh}$ (=1) is the stoichiometric factor for CO chemisorption, V$_{CO}$ (cm$^3_{STP}$·g$_{cat}$$^{-1}$) is the amount of CO chemisorbed on Rh, M$_{Rh}$ (=102.91 g mol^{-1}) is the molar mass of Rh, L$_{Rh}$ (=0.006) is the Rh content in the catalyst.

On the same apparatus, the reduction proprieties of the samples were measured by H$_2$ temperature-programmed reduction (H$_2$-TPR). The samples were heated from −80 °C up to 1020 °C at a rate of 20 °C min^{-1} in a 5% H$_2$/Ar (30 Nml min^{-1}) mixture. Before the experiments, the samples were heat treated under O$_2$ flow (30 Nml min^{-1}) at 200 °C for 1 h and cooled down to sub-ambient

Table 1

Textural and structural properties of synthesized CeO_2 and Rh/CeO_2 samples by XRD, CO-chemisorption and TEM analysis.

Sample	Rh content[a] (wt.%)	SA_{BET} (m^2/g)	XRD		CO-chemisorption		TEM
			CeO_2 Lattice parameter[b] (nm)	CeO_2 Particle size[b] (nm)	Rh Particle size[c] (nm)	Rh Dispersion[c] (%)	Rh Particle size (nm)
CeO_2	–	65.2	0.5394	15.1	–	–	–
Rh/CeO_2	0.57	31.0	0.5386	21.9	5.8	18.9	2–4

[a] Determined by ICP/OES chemical analysis.

[b] Calculated from X-ray diffraction: CeO_2 lattice parameter (α) from the relation $\alpha = \sqrt{h^2 \cdot k^2 \cdot l^2} \cdot \left(\lambda/2 \cdot \sin\theta \right)$; CeO_2 crystallite size from the Sherrer equation of the CeO_2 (111) reflection.

[c] Determined by CO-chemisorption through the Takeguchi method [21].

temperature ($-80\,°C$) under inert atmosphere (He) to remove any moisture present. The hydrogen consumption was monitored by a TCD detector and the response was quantitatively calibrated from the H_2-TPR area of known amounts of CuO.

Transmission electron microscopy (TEM) images of fresh and spent catalysts were obtained using a *Philips CM12* instrument. Powder samples were dispersed on holey copper grids after sonication in isopropyl alcohol. 5 images (ca. 120 particles) were collected per sample and analyzed by Image J software.

Temperature-programmed oxidation (TPO) measurements were carried out in order to estimate the amount carbon generated during SR tests. The samples were heated from ambient temperature up to $1000\,°C$ at a rate of $10\,°C\,min^{-1}$ in a He flow ($30\,Nml\,min^{-1}$). The CO_2 production was monitored by a quadrupole mass spectrometer (*QMS Thermo Scientific ProLab*) and the response was quantitatively calibrated from the TPO area of known amounts of $CaCO_3$.

2.3. Catalytic tests

A detailed description of the experimental setup as well as mass balance calculations of both reactant and product mixtures were provided in a previous publication [13]. Briefly, the catalytic performance of Rh/CeO_2 catalyst was tested in a fixed-bed reactor (i.d. = 0.8 cm) using the temperature-controlled bed configuration previously studied. Indeed, the temperature of the catalytic bed increased from ca. $500\,°C$ (T_{IN}) to $800\,°C$ (T_{SET}), avoiding carbon formation due to *n*-dodecane cracking phenomena. 0.6 g of catalyst diluted in 0.6 g of quartz were used in each test. *N*-dodecane (Aldrich) was selected as surrogate for diesel fuel. Thiophene (Aldrich) was added as model compound of organic sulfur naturally present in commercial diesel fuel.

Stability tests of sulfur-free *n*-dodecane SR were performed over 100 h of time-on-stream by sequential start-up and shutdown cycles of ca. 6 h, varying the steam-to-carbon molar ratio (S/C = 1–2.5) at fixed space velocity (GHSV = 16,000 h^{-1}, as gas hourly space velocity of gases fed at $0\,°C$ and 1 bar per volume of catalyst). Additional tests were carried out at S/C = 1 and higher space velocity (GHSV = 40,000 h^{-1}) until catalyst deactivation. In between each cycle, the reactor was cooled to ambient temperature under N_2 flow. Then, the regeneration step was carried out by re-increasing the temperature to $800\,°C$ under air flow. The regeneration was stopped once the CO_2, due to the combustion of carbon deposits, was detected below 1 vol.%.

Stability tests of sulfur-containing *n*-dodecane were performed over 50 h of time-on-stream at GHSV = 16,000 h^{-1} and S/C = 1.5. The sulfur concentration (30, 60 and 100 ppm) was selected to simulate or exceed the sulfur content (<50 ppm) in commercial diesel for automotive application in European Community's countries [22]. Particularly, the high sulfur concentrations (50 and 100 ppm) were used to accelerate catalyst deactivation. The role of steam
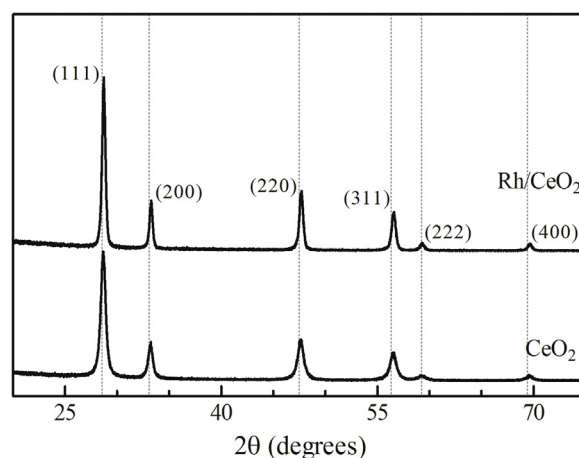

Fig. 1. XRD patterns of CeO_2 support and Rh/CeO_2 catalyst (JPDS 4-593 reference peaks of CeO_2 also included as dotted lines).

in reducing the effect of sulfur poisoning was further investigated increasing the S/C ratio up to 2.5.

Results were reported as molar concentrations of H_2, CO, CO_2, CH_4 and by-products (C_2H_6, C_2H_4, C_3H_8, C_3H_6) and H_2/CO molar ratio. Chemical compositions in thermochemical equilibrium were derived using the *HSC Chemistry 7.1*® calculation software. This software gives the equilibrium vapour pressures of the existing species ($C_{12}H_{26}$, CH_4, O_2, H_2O, CO_2, CO, H_2, solid carbon) using the Gibbs free-energy minimization procedure.

3. Results and discussion

3.1. Characterization of fresh Rh/CeO_2 catalyst

The characteristic properties of the synthesized samples are shown in Table 1. The as prepared CeO_2 support and Rh/CeO_2 catalyst showed BET surface area of ca. 65 and 31 m^2/g, respectively. X-ray diffraction patterns in Fig. 1 showed well-defined peaks that can be indexed to the face-centered cubic phase of CeO_2. Characterization peaks at 2θ of 28.55, 33.08, 47.50, 56.33, 59.26 and 69.41 were observed. However, no diffraction peaks due to Rh oxides could be detected, probably due to the low metal loading and to the fact that Rh species are highly dispersed on the support. The average crystallite size calculated from the Scherrer equation using the (111) peak was found to be 15.1 and 21.9 nm for CeO_2 and Rh/CeO_2, respectively (Table 1). SCS is a self-sustained chemical process, which takes place in a homogeneous solution of precursors and fuel [23–25]. As previously reported [20], the nature of precursors and fuel and the fuel-to-oxidant ratio affect the flame temperature generated during combustion and the moles of produced gases, having a strong influence on the morphological properties of the synthesized powders. Indeed, the higher flame temperature recorded for
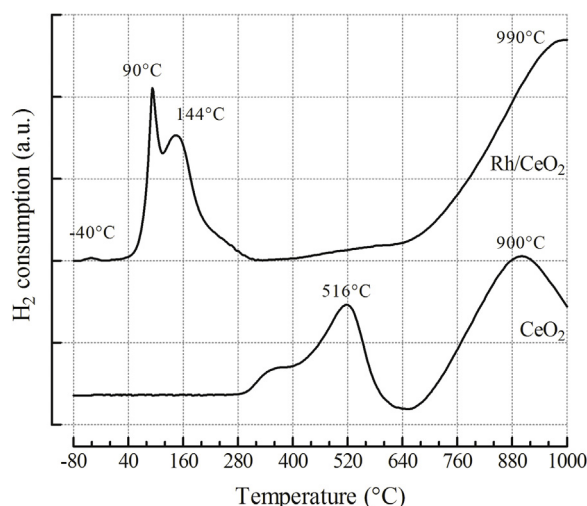
Fig. 2. H_2-TPR patterns of CeO_2 and Rh/CeO_2 samples.

the Rh/CeO_2 catalyst led to lower surface area ($31\,m^2/g$) and higher crystallite size (21.9 nm) compared to the values of bare CeO_2 support ($65\,m^2/g$ and 15.1 nm, respectively). Moreover, the analyses of lattice parameter revealed that the value decreased with introducing the Rh metal phase (Table 1). The pure CeO_2 support had a lattice parameter of 0.5394 nm, while the Rh/CeO_2 catalyst had a lattice parameter of 0.5386 nm. This indicated the partial substitution of Ce^{4+} (0.097 nm) with smaller Rh^{3+} (0.068 nm) ions, resulting in the shrinkage of the CeO_2 cell due to the formation of Ce-Rh-O solid solution.

Additionally, from the data obtained by means of pulse CO-chemisorption technique, the calculated metallic dispersion was 18.9%, corresponding to Rh particle diameter of 5.8 nm.

In Fig. 2, the TPR profiles of catalyst and support are presented. CeO_2 sample showed two main reduction peaks at 516 and 900 °C, respectively. As reported in literature, the low-temperature peak was due to the reduction of CeO_2 surface oxygen, while the high-temperature peak was due to CeO_2 bulk oxygen reduction [26,27]. The reduction profile of Rh/CeO_2 took place in four stages, with maximum temperature peaks at −40, 90, 144 and 990 °C. The peak at sub-ambient temperature was previously ascribed to the reduction of the readily available surface oxygen adjacent to the metal, indicating the presence of well dispersed rhodium oxide species with uniform particle size distribution [28,29]. According to Djinović et al. [30], the peaks at 90 and 144 °C could be assigned to the reduction of Rh_2O_3 to metallic Rh and the reduction of CeO_2 surface oxygen, respectively. It is well known that the presence of transition as well as noble metals on the catalyst surface induces extensive changes in the reduction profile of ceria [30–32]. Indeed, CeO_2 surface oxygen reduction (144 °C) shifted towards lower temperature than the bare ceria (510 °C) due to the presence of Rh. This assumption could be explained by the strong metal-support interaction (SMSI) provided by the synthesis method, as well as by the Ce-Rh-O solid solution formation observed during XRD analysis [33,34]. The quantification of hydrogen consumption related to the peaks at −40 and 90 °C ($0.0758\,mmol_{H2}\,g_{cat}^{-1}$), was almost equal to that required for the complete reduction of Rh_2O_3 to metallic Rh ($0.0831\,mmol_{H2}\cdot g_{cat}^{-1}$), corresponding to a reduction degree of 91.2%. The theoretical hydrogen consumption was calculated according to the actual chemical composition of the catalysts, equal to 0.57 wt.% as determined from ICP/OES chemical analysis (Table 1). Consequently, the quantity of consumed H_2 at 144 °C ($0.1510\,mmol_{H2}\,g_{cat}^{-1}$), corresponded to the partial reduction of 5.2% of total adjacent CeO_2 to Ce_2O_3, as a result of hydrogen spillover mechanism due to the presence of Rh. This is very likely

due to the easy H_2 dissociation on Rh, followed by spillover of H species onto CeO_2 [14,35,36]. Finally, the high-temperature zone (maximum at 990 °C) was ascribed to CeO_2 bulk oxygen reduction, which does not seem affected by Rh presence.

TEM image in Fig. 3 showed the morphology of the Rh-based catalyst. The observed Rh particles sizes were ca. 2–5 nm, which were well consistent with the CO chemisorption (Table 1) and TPR (Fig. 2) results.

As reported by Voskanyan and co-workers in a recent review [37], the high temperature required for crystal nucleation is achieved by the self-generated heat, while the rapid cooling (few minutes) avoid the crystal growth. Thus, nanosize crystalline metal oxides were produced by solution combustion method. The characterization results of the Rh/CeO_2 catalyst suggested that CeO_2 crystallite sizes of ca. 20 nm were obtained. At the same time, highly dispersed system was synthesized, with Rh sizes of ca. 2–5 nm, as evidenced by CO-chemisorption and TEM analysis. Moreover, XRD patterns highlighted the formation of the Ce-Rh-O solid solution coupled with a SMSI as revealed from TPR results.

3.2. SR of sulfur-free n-dodecane

3.2.1. Stability tests at various S/C ratios

The effect of the S/C molar ratio on the catalytic stability was studied in order to explore the appropriate coke-free reaction conditions. It is well known that the large carbon content constitutes one of the main concerns in steam reforming of heavy hydrocarbon fuels [38]. The effectiveness of the catalyst can significantly decrease due to coking phenomena. Particularly, graphitic carbon is more difficult to eliminate and can block active sites of the catalyst, determining a progressive reduction of the catalytic activity. Generally, coke formation can be suppressed by optimizing the steam content in the reactant mixture [38,39].

Fig. 4 shows the influence of the S/C ratio (from 2.5 to 1) on the activity of Rh/CeO_2 catalyst at GHSV = 16,000 h^{-1} over 100 h of time-on-stream. A comparison between equilibrium predictions (dotted lines) and experimental data was also reported. It can be seen that products concentration agreed well with the equilibrium calculations. However, at all the investigated S/C ratios, CO_2 and H_2O concentrations were higher, while CO concentration was lower than the predicted equilibrium values. It is important to consider that equilibrium values were calculated at 800 °C, while a temperature gradient (500–800 °C) was employed along the catalytic bed. As previously reported [13,40], the contribution of exothermic water gas shift (WGS) and methanation equilibriums was more relevant than the predictable values (at 800 °C). Indeed, WGS ($CO + H_2O = CO_2 + H_2$, $\Delta H°_{298} = -206.2\,kJ\,mol^{-1}$) and methanation ($CO_2 + 4H_2 = CH_4 + 2H_2O$, $\Delta H°_{298} = -165.0\,kJ\,mol^{-1}$) reactions could be favoured in the first part of the catalytic bed at lower temperature. Since H_2O and CO_2 are involved in both equilibriums, the composition of the product mixture depends on the contribution of the individual reactions. In addition, comparing the activity of the Pt/CeO_2 catalyst at S/C = 2.5 previously reported [13], with that of the Rh/CeO_2 catalyst, it is possible to note that the contribution of WGS reaction was more pronounced on the Pt-based catalyst. This could be probably ascribed to the nature of the Pt active sites, which displayed higher intrinsic selectivity towards CO and H_2O in comparison to Rh metal phase [41,42].

Rh-based catalyst showed stable catalytic activity at S/C = 2.5 with H_2 concentration of ca. 50% (N_2-free basis), accompanied by a H_2/CO ratio of ca. 4. The high catalytic activity was evidenced by the absence of by-products, while for the Pt/based system low concentrations of CH_4 and C_2H_4, equal to 0.2% and 0.1% respectively, were observed after 34 h of time-on-stream, as previously reported [13]. Decreasing the S/C to 1.5, the activity of Rh/CeO_2 remained stable, while H_2 concentrations increased to ca. 60%. Similarly, CO
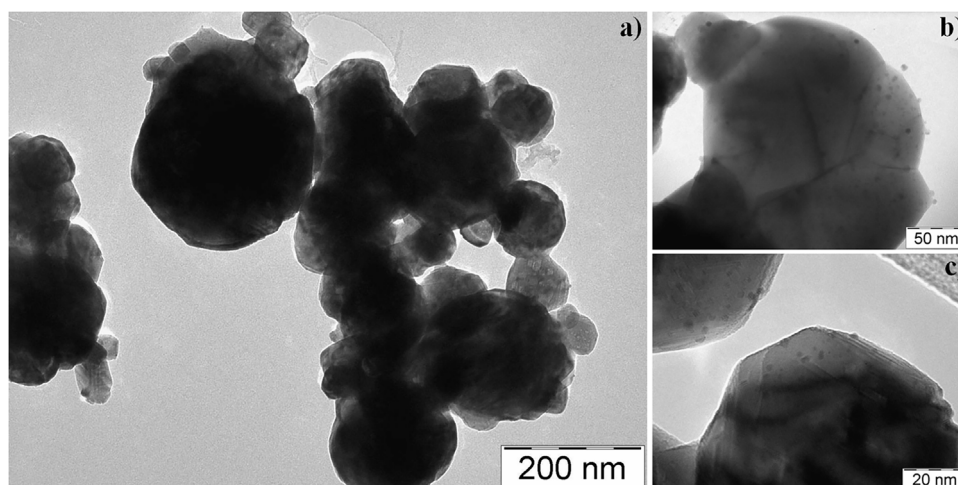
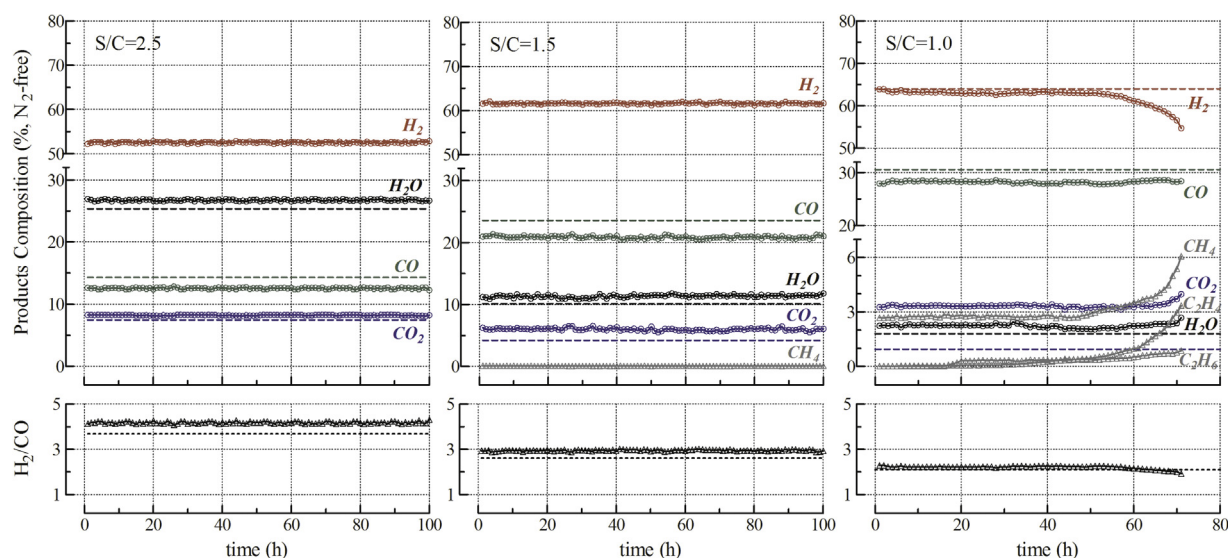**Fig. 3.** TEM images of the as prepared Rh/CeO_2 catalyst.

Fig. 4. Products composition (N_2-free basis) and H_2/CO ratio as a function of time. SR stability tests of sulfur-free *n*-dodecane at different S/C ratio (GHSV = 16,000 h^{-1}; 500–800 °C temperature gradient).

concentration increased from 12 (S/C = 2.5) to 20% (S/C = 1.5), leading to a decrease in the H_2/CO molar ratio from 4 (S/C = 2.5) to 3 (S/C = 1). On the contrary, significant catalyst deactivation was observed at S/C = 1 after 50 h of time-on-stream. In this condition, H_2 concentration decreased from the equilibrium value (ca. 65%) to 55%. Catalyst deactivation led to increased production of by-products, as methane (6.1%), ethane (0.9%) and ethylene (3.3%) (Fig. 4).

Additional tests were carried out at S/C = 1 and higher space velocity (GHSV = 40,000 h^{-1}) to study the regeneration capability of the catalytic system and the results are presented in Fig. 5. It should be noted that the low S/C ratio and the high GHSV values were selected in order to enhance catalyst deactivation, which was essential to study the regeneration of the catalyst after coke combustion with air. The activity of the Rh/CeO_2 catalyst remained stable for ca. 40 h of time-on-stream, decreasing afterwards. A progressive decrease in H_2 concentration from ca. 63.4–54.5% was observed, as well as the increase in by-products concentrations, mainly CH_4 (7.6%) and C_2H_4 (2.2%). The regeneration step, carried out under air flow, allowed to restore the initial activity, due to the removal of carbon deposits as CO_2 revealed on TCD detector (not shown). Deactivation/regeneration cycles were repeated and
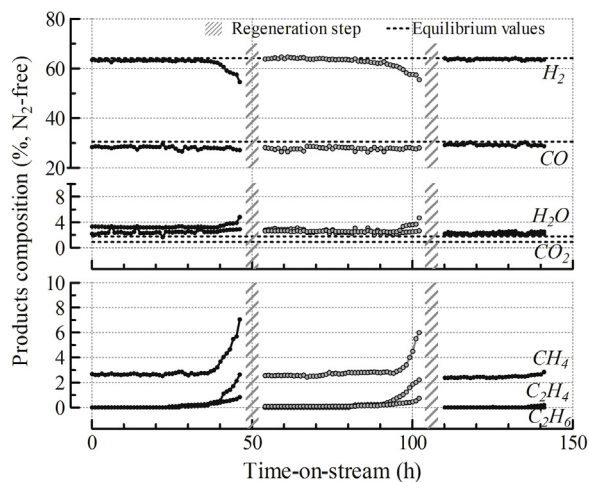

Fig. 5. Products composition (N_2-free basis) as a function of time. SR regeneability test of sulfur-free *n*-dodecane (S/C = 1; GHSV = 40,000 h^{-1}; 500–800 °C temperature gradient).
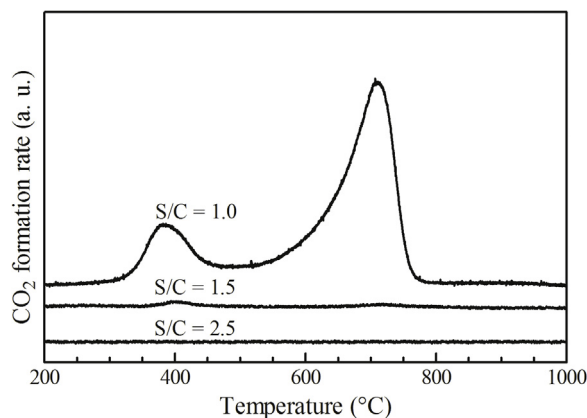
Fig. 6. TPO profiles of used Rh/CeO_2 catalyst. Effect of the S/C ratio on the CO_2 formation.

also in this case the initial products concentration was restored, indicating that full catalyst regeneration was possible (Fig. 5).

It is important to note that two aspects need to be considered to evaluate the regeneration capability, namely (i) the restoring of the initial activity and (ii) the duration of the stability period after air treatment. Indeed, although the air treatment is an economic and environmental friendly way to regenerate the catalyst, the initial activity could not be recovered and/or the deactivation after air treatment could occurr more rapidly. Simons et al. [43] found that the regeneration treatment in air at 650 °C allowed restoring the initial activity of Rh/Pt-based catalyst by removing the carbon species deposited during the steam reforming of ethanol/gasoline mixtures. However, the deactivation following the air treatment occurred more rapidly than the fresh catalyst [43]. Similar results were reported by Roh et al. [44] towards ethanol steam reforming with $Rh/CeO_2–ZrO_2$ catalyst. Moreover, the Pt/CeO_2 system previously studied completely restored the activity but a more rapid deactivation behaviour was observed [13]. On the contrary, an interesting result was obtained with the Rh/CeO_2 catalyst, for which the activity profile of the regenerated catalyst corresponded, both in terms of composition and duration, with that of the fresh catalyst (Fig. 5).

3.2.2. Characterization of the used catalysts

Temperature-programmed oxidation (TPO) of deposited carbon was performed to understand both the quantity and the quality of coke formed on the three different types of spent samples. Fig. 6 shows the TPO profiles of Rh/CeO_2 catalysts after stability tests at different S/C ratio. At high S/C ratio (S/C = 1.5, 2.5) no carbon formation was revealed. As expected, this result confirmed the high resistance of the Rh/CeO_2 catalyst, due to the high C—C bond breaking capacity of Rh metal phase and the high oxygen mobility of CeO_2 support, as widely reported [45–48].

Contrarily, at low S/C ratio (S/C = 1) two peaks appeared on the TPO pattern. The first peak centered at ca. 385 °C was less pronounced and could be attributed to the formation of more reactive amorphous carbonaceous species located at metal/support interfaces [49,50]. The more intense high-temperature peak (centered at 710 °C) was ascribed to the formation of less reactive graphitic species principally deposited on the support [51,52]. Similar results were reported by Chen et al. [53] for the catalytic decomposition of isoctane at 725 °C; the TPO measurements evidenced two peaks at 382 and 638 °C of which the peak at low temperature was assigned to the oxidation of reactive coating carbon while the peak at high temperature was ascribed to the oxidation of less reactive filamentous carbon.

The quantification of TPO pattern indicated a carbon formation rate of 0.08 $mmol_C$ g_{cat}^{-1} h^{-1} (corresponding to ca. 7.2 wt.% C). The amount of carbon accumulation depend on the balance between carbon formation reactions (cracking of C—H bonds, Boudouard reaction and reverse gasification) and carbon removal reactions (gasification, reverse Boudouard reaction and carbon methanation) [54]. At low S/C ratio (S/C = 1), the amount of carbon could increase due to the low concentration of H_2O, which mainly limited the gasification reaction. Moreover, less CO was converted by the water gas shift reaction, becoming available for carbon production by the Boudouard reaction as suggested by Reitmeier et al. [55]. Moreover, the high carbon content was confirmed by the presence of ethylene (Fig. 4) that is reported to be the main reason for rapid carbon formation in the reforming process [56].

Fig. 7 shows the TEM images of the Rh/CeO_2 catalyst used at S/C = 1. Different types of carbon specie were identified (Fig. 7a). In particular, amorphous and graphitic carbon, corresponding to the low-temperature and high-temperature peaks in TPO pattern (inserted Figure), were observed. The morphological structure appeared to be similar to that of the fresh catalyst (Fig. 3a), since no evidence of support agglomeration was observed. Moreover, Rh particles dispersion was almost uniform with metal sizes ranging from 4 to 9 nm (Fig. 7b,c). The good anti-sintering ability of the catalyst could be related to the SMSI, since the high resistance force caused by this interaction made difficult the transfer of Rh particles on the CeO_2 support [57,58].

To shed light on the nature of carbonaceous deposits, further TEM investigation was done after treating the used sample in air at 500 °C in order to burn off the fraction of the amorphous carbon present on the catalyst. TEM images of the air treated sample (Fig. 7d) showed two types of graphitic carbon, as revealed from the high-magnification of carbon deposits (Fig. 7e,f), evidencing the basal planes of the crystalline graphite. The carbon species related to the high-temperature peak in TPO profile, could be ascribed to the presence of both pyrolitic and filamentous carbon, as previously resported in Rostrup-Nielsen's review [59]. It is important to note that the filamentous carbon species were not attached to Rh particles as well as encapsulatic carbon deposits were not observed, which are the main cause of catalyst deactivation [58,60]. Thus, three types of carbon deposits were identified in steam reforming of n-dodecane at S/C = 1, namely amorphous, filamentous and pyrolytic carbon (Fig. 7a). As widely reported, both the typology of carbon formed during reforming reaction and the sinthering phenomenon strongly depend on the nature and the strenght of the metal-support interaction, determining the good stability and high coke-resistence of the Rh/CeO_2 catalyst.

Finally, the addition of steam favoured the catalyst performance dramatically reducing the carbon deposition phenomena. However, higher amount of steam means higher energy requirements, that lowers the overall process efficiency [61]. Hence, in order to maximize the catalyst performance while minimizing the energy consumption, S/C = 1.5 was selected as reaction condition for subsequent experiments in the presence of sulfur.

3.3. SR of sulfur-containing n-dodecane

3.3.1. Stability tests with various sulfur content

Reforming experiments were performed at three different sulfur concentrations, namely 30, 60 and 100 ppm S. Fig. 8 shows the product gas composition and the H_2/CO ratio during steam reforming of sulfur-containing n-dodecane at S/C = 1.5 and GHSV = 16,000 h^{-1}. In all cases, a slight decrease in catalytic performance, in term of H_2 concentration, was observed. Besides, the decrease in catalytic activity became more pronounced by increasing the sulfur concentration in the feed, as evidenced in Fig. 9, comparing the relative H_2 yield, as ratio between the H_2 produced to the initial value.
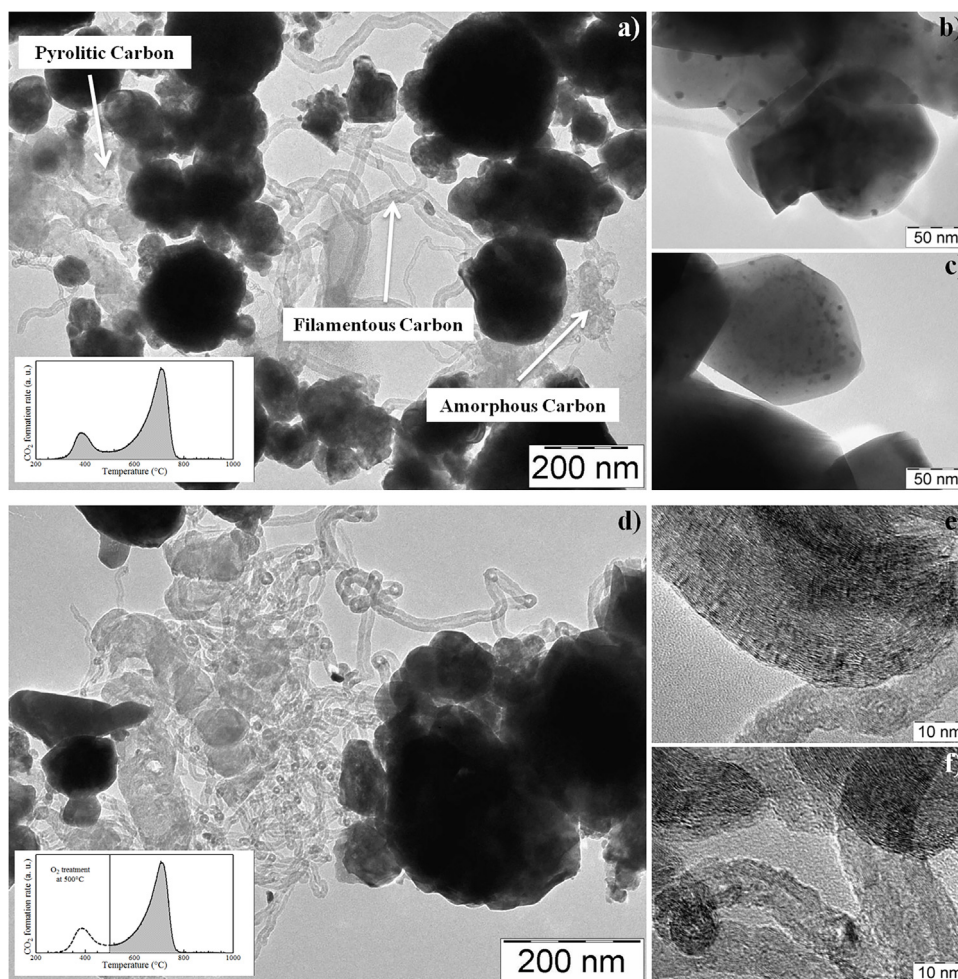
Fig. 7. TEM images of the Rh/CeO_2 catalyst after SR of sulfur-free *n*-dodecane at S/C = 1.
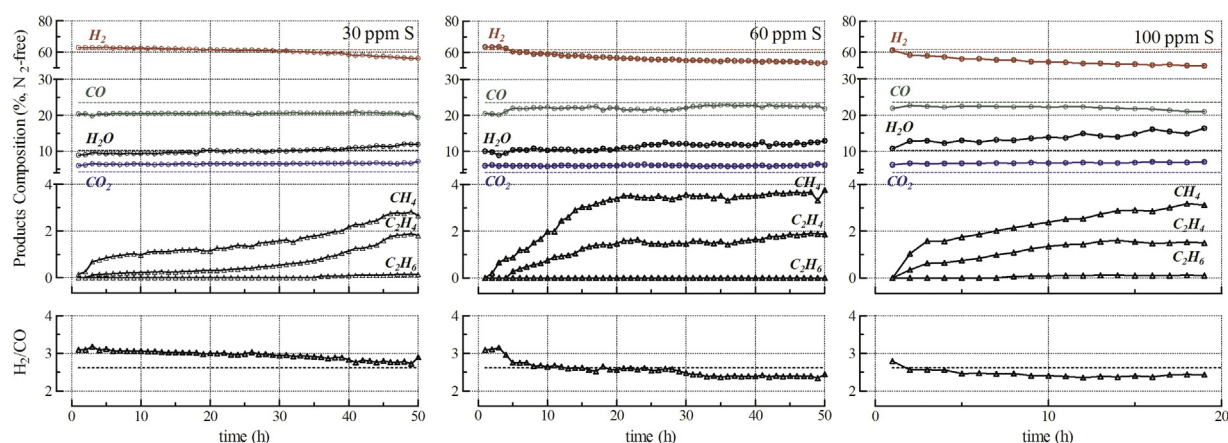

Fig. 8. Products composition (N_2-free basis) and H_2/CO ratio as a function of time. SR stability test of sulfur-containing *n*-dodecane at different sulfur content (S/C = 1.5; GHSV = 16,000 h^{-1}; 500–800 °C temperature gradient).

The effect of sulfur content on the relative H_2 yield is shown in Fig. 9a, in which a reduction in H_2 production of 12% was determined for the 30 ppm sulfur feed after 50 h of test, while no H_2 reduction was obtained in absence of sulfur at S/C = 1.5 (Fig. 9a). Meanwhile, the formation of by-products increased as a function of time-on-stream, leading to ca. 4 and 3% of methane and ethylene, respectively (Fig. 8). Higher sulfur concentrations led to a faster deactivation: higher reduction in H_2 production (ca. 16 and

17% at 60 and 100 ppm S, respectively) was observed along with a greater amount of by-products, mainly methane and ethylene (Fig. 8). Moreover, the test at 100 ppm S was stopped after ca. 20 h of time-on-stream, due to high pressures recorded at the inlet of the reactor, related to the high quantity of carbon deposits.

A significant improvement in the sulfur tolerance was observed increasing the steam content. Fig. 9b compares the results obtained for 100 ppm sulfur feed at various S/C ratio. At S/C = 2.5 a lower
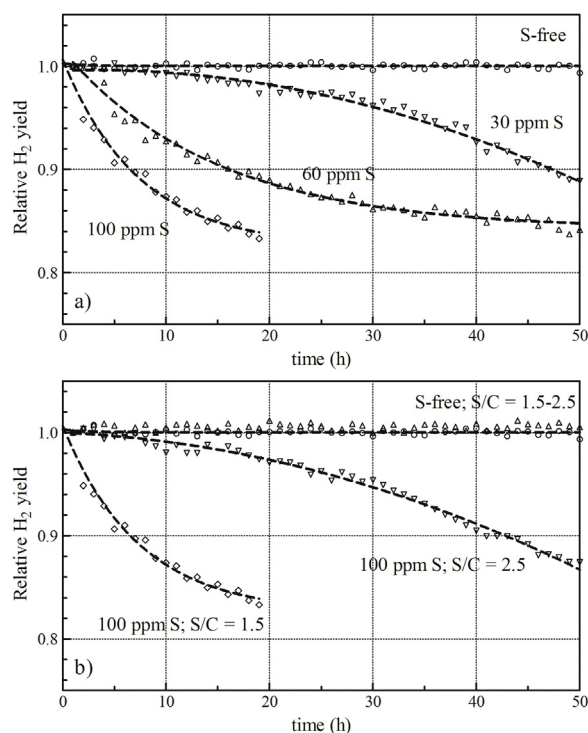
Fig. 9. Relative H_2 yield as a function of time. SR stability tests at (a) different sulfur content (S/C = 1.5; GHSV = 16,000 h^{-1}) and (b) S/C ratio (100 ppm S; GHSV = 16,000 h^{-1}).
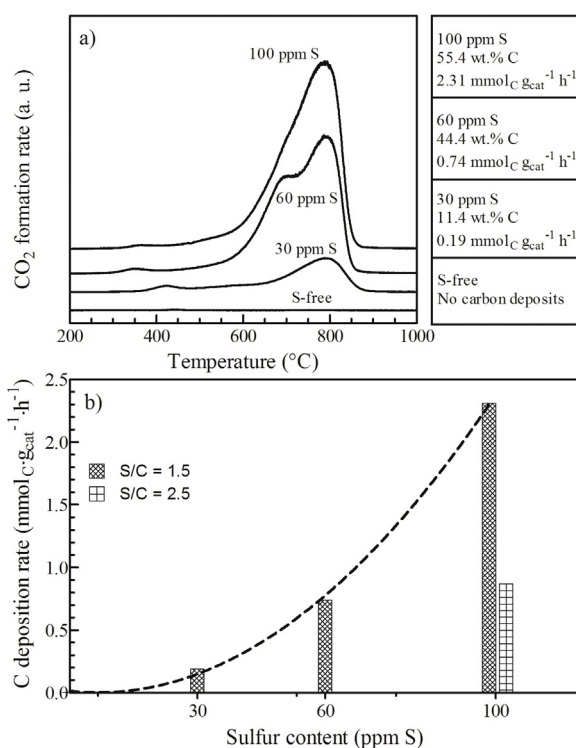

Fig. 10. TPO profiles of used Rh/CeO$_2$ catalyst. Effect of the sulfur content on (a) CO$_2$ formation rate and (b) C deposition rate.

reduction in H$_2$ production (ca. 13% after 50 h of reaction) was found, compared to the value obtained at S/C = 1.5 (ca. 17% after 19 h of reaction). Moreover, higher S/C ratio led to lower by-products content in the product mixture (not shown). Similar results were reported by Ferradon et al. [62], which investigated the effect of the steam-to-carbon ratio during reforming of low-sulfur (34 ppm) gasoline over a Rh/La-Al$_2$O$_3$ catalyst. They determined significantly different amounts of deposited carbon on the used catalyst at S/C of 2.0 (44.6 wt.%) and S/C of 3.0 (2.99 wt.%). The inability of the catalyst to promote the gasification of carbon was the main cause of deactivation, while the beneficial effect of the steam content on sulfur tolerance was due to the regeneration capacity of steam in combination with H$_2$ [62]. Indeed, steam favours the removal of sulfide species and the gasification of coke, leading to a regeneration of the catalyst surface, as previously reported by other Authors [53–65]. However, the enhanced sulfur tolerance by increasing the S/C is accompanied by an energy penalty due to higher energy consumption in steam vaporization. We calculated additional 730 kJ/h at S/C of 2.5 compared to S/C = 1.5 per mol/h of *n*-dodecane fed. Consequently, S/C ratio should be minimized for energy efficiency [62].

3.3.2. Characterization of the used catalysts

Fig. 10a shows the TPO profiles of Rh/CeO$_2$ catalysts after 50 h stability test at different sulfur concentration (30, 60 and 100 ppm S). The TPO profile at S/C = 1.5 under sulfur-free condition is also reported for comparison. As first evidence, excessive carbon deposition was revealed during sulfur-doped runs, while no carbon formation was observed in absence of sulfur. Moreover, the presence of sulfur promoted the formation of less reactive graphitic carbon, since only a main peak at high temperature (ca. 790°) was evidenced [66]. The quantity of carbon deposit significantly increased by increasing the sulfur content, as evidenced in Fig. 10b. At 30 ppm sulfur feed the carbon formation rate was 0.19 mmol$_C$ g$_{cat}$$^{-1}$ h^{-1} (corresponding to ca. 11.4 wt.% C).

Increasing sulfur to 60 and 100 ppm, the carbon deposition rate was 0.74 mmol$_C$ g$_{cat}$$^{-1}$ h^{-1} (corresponding to ca. 44.4 wt.% C) and 2.31 mmol$_C$ g$_{cat}$$^{-1}$ h^{-1} (corresponding to ca. 55.4 wt.% C), respectively. A close relation between the cracked products in the reformate (Fig. 8) and the amount of carbon deposition was also revealed. Similar results were reported by other Authors, obtaining increased amounts of carbon deposits in the presence of sulfur during steam reforming of liquid fuels over Rh-based catalysts [15,66,67].

As expected, the TPO pattern of the catalyst used with 100 ppm sulfur feed at S/C = 2.5 (not shown) indicated a significant reduction of the deposited carbon species, leading to a lower carbon formation rate (0.87 mmol$_C$ g$_{cat}$$^{-1}$ h^{-1}) compared to the test carried out at S/C = 1.5 (2.31 mmol$_C$ g$_{cat}$$^{-1}$ h^{-1}) (Fig. 10b).

As reported by Lakhapatri et al. [15], the low temperature peak is typically assigned to coke deposited in the vicinity of metal particles while the high temperature peak is attributed to the carbon in close contact with the support. Since only the high-temperature peak was present, it could be deduced that carbon deposition on Rh-CeO$_2$ catalyst in the presence of sulfur mainly occurred on the support.

The TEM images of the post-reformed (100 ppm Sulfur feed) catalyst are shown in Fig. 11, evidencing a high carbon content (Fig. 11a), as revealed from TPO results. The high-magnification of carbon deposits (Fig. 11b) evidenced the basal planes of the crystalline graphite, corresponding to the high-temperature peak in the relative TPO pattern (Fig. 10). Despite the large amount of carbon deposits, carbon-free and well dispersed Rh sites were observed, as shown in Fig. 11c.

3.3.3. Effect of sulfur on SR of n-dodecane

It has been recently demonstrated that Rh-based catalysts suffer from sulfur poisoning during SR processes, but contradictory results are present in literature on the deactivation mechanism. It is well know that most of the organosulfur contained in the hydrocarbon fuels converts to H$_2$S at low temperatures (300–400 °C) in
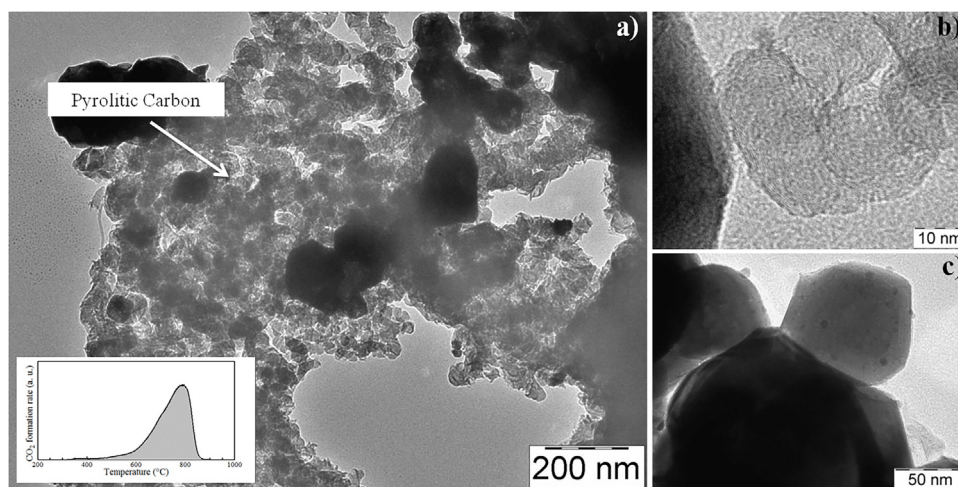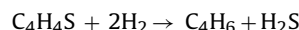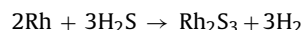
Fig. 11. TEM images of the Rh/CeO$_2$ catalyst after SR of 100 ppm sulfur-containing n-dodecane at S/C = 1.5.

non-oxidizing atmosphere [68,69]. H$_2$ produced during the early stages of steam-reforming acts as a hydrodesulfurization precursor, converting the organosulfur into H$_2$S:
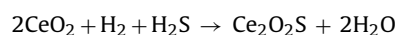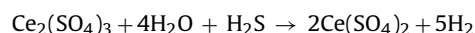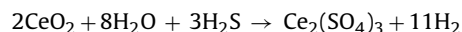
$$C_4H_4S + 2H_2 \rightarrow C_4H_6 + H_2S$$

H$_2$S can selective adsorbs to metal sites to form metal-sulfur bonds, inhibiting the hydrocarbon chemisorption and reducing the catalyst activity [70,71]. Azad and Sundararajan [72] proposed for a Rh-based catalyst the following deactivation mechanism:

$$2Rh + 3H_2S \rightarrow Rh_2S_3 + 3H_2$$

in which, H$_2$S derived from thiophene could react with nanoscale Rh, partially producing Rh$_2$S$_3$, the most stable rhodium sulfide. Since any evidence of carbon deposition was found, they attributed the loss of activity to the sulfur poisoning of the metal phase, indicated as the main cause of catalyst deactivation. Lakhapatri et al. [15] demonstrated that sulfur adsorbed on the metal phase of Rh-Ni/Al$_2$O$_3$, preferentially forming the more stable Ni-S bond. Consequently, the hydrocarbons adsorbed on the sulfur-poisoned active sites migrated to the nearby support surface where they underwent acid site cracking, accumulating as aromatic or polymeric species.

Differently, H$_2$S can increase the surface acidity due to the presence of oxysulfides, disfavoring the coke gasification by suppressing the dehydrogenation reactions [73–75]. Laosiripojana at al. [74] reported a contradictory effect of H$_2$S related to the formation of various Ce-O-S phases:

$$2CeO_2 + 8H_2O + 3H_2S \rightarrow Ce_2(SO_4)_3 + 11H_2$$

$$Ce_2(SO_4)_3 + 4H_2O + H_2S \rightarrow 2Ce(SO_4)_2 + 5H_2$$

$$2CeO_2 + H_2 + H_2S \rightarrow Ce_2O_2S + 2H_2O$$

The Authors revealed that Ce(SO$_4$)$_2$ promoted the OSC of ceria, while the Ce$_2$O$_2$S phase reduced the lattice oxygen mobility, negatively affecting the reforming activity [74]. Cheekatamarla et al. [75] presented the results of the degradation processes over a 1% Pt/CeO$_2$ catalyst for the autothermal reforming (ATR) of diesel, highlighting the sulfur poisoning mechanism. They attributed the activity loss to the diffusion of certain poisoning compounds, namely carbon and sulfate/sulfites, on the CeO$_2$ support. Moreover, Ferriz et al. [76] determined the favourable thermodynamic conditions to obtain stable Ce$_2$O$_2$S. The phase diagram suggested that

the ceria catalyst should not be seriously affected at more modest sulfur levels (<100 ppm) in the fuel.

The Rh/CeO$_2$ catalyst proposed in this study did not show very pronounced loss of activity in term of H$_2$ production (Figs. 8, 9), but large amounts of deposited carbon were observed over the used catalysts (Fig. 10), especially at high sulfur content. Moreover, the position of the TPO peaks indicated that the main cause of deactivation in the presence of sulfur occurred on the support of the catalyst. In addition, carbon-free and well dispersed Rh sites were observed, as evidenced by TEM images (Fig. 11) and further confirmed by the absence of low-temperature peak in TPO measurements (Fig. 10) that is generally attributed to carbon species deposited near metal particles. Indeed, free Rh atoms could still be able to activate the hydrocarbon molecules. This could explain the catalytic activity obtained during 50 h of time-on-stream, which remained quite high in spite of the considerable amount of deposited carbon.

Therefore, coking seems to be the main deactivation mechanism in the SR of sulfur-containing n-dodecane and it was promoted by increasing the sulfur concentration. Low sulfur concentration was evidenced by CHNS analysis, determining ca. 220 ppm of total sulfur in the sample used with high sulfur content (100 ppm S). The formation of Rh sulfide could explain the loss of activity observed in Fig. 9, allowing for thermal cracking reactions of the hydrocarbon adsorbed on the sulfur-poisoned active phase and migrated to the support surface [15,72]. Indeed, huge amounts of pyrolitic carbon were found on the support, as evidenced in TEM (Fig. 11) and TPO (Fig. 10) analysis, justifying the thermal cracking mechanism. However, partial deactivation due to oxysulfides formation on the CeO$_2$ support could not be excluded, especially at high sulfur content (100 ppm S) that favoured Ce2O2S formation, as reported by Ferriz et al. [76]. The presence of oxysulfides increased the surface acidity and suppressed, in turn, the carbon gasification by hindering the steam dissociation into highly reactive surface oxygen species (O and OH), lowering their mobility on the catalyst surface and inhibiting the interactions between carbon deposits and the surface oxygen species [57]. The beneficial effect of steam in removing the sulfide specie and favoring the gasification of coke, led to improved sulfur tolerance of the Rh/CeO$_2$ catalyst for the steam reforming of sulfur-containing n-dodecane.

4. Conclusions

The solution combustion synthesized 0.6 wt.% Rh/CeO$_2$ catalyst showed an outstanding catalytic activity for the steam reforming of sulfur-free n-dodecane, mainly due to the high metal

dispersion and the strong metal-support interaction. Higher S/C ratio positively favoured catalyst stability, while simultaneously reducing carbon deposition. Constant H_2 concentration (62%, N_2-free basis) in the product mixture and absence of carbon deposition were observed at S/C = 1.5 for 100 h of time-on-stream. Moreover, successive deactivation/regeneration cycles indicated that full catalyst regeneration was possible. The nature and the strenght of the metal-support interaction determined the good anti-sintering ability and the high coke-resistance of the Rh/CeO$_2$ catalyst.

The presence of sulfur enhanced the carbon deposition rate, which was the main cause of catalyst deactivation. The formation of Rh sulfide allowed the migration of adsorbed hydrocarbons to the CeO$_2$ support, where they undergo thermal cracking, accumulating as pyrolitic species. Moreover, the increased surface acidity, due to the presence of oxysulfides species on the CeO$_2$ support (at high S content), hindered coke gasification reaction, inhibiting the interactions between carbon deposits and the surface oxygen species. Higher steam content improved the gasification of carbon and the sulfur resistance of the Rh/CeO$_2$ catalyst for the steam reforming of *n*-dodecane.

Characterization data and reforming results of the low-loaded Rh/CeO$_2$ catalyst made it a promising active/stable and low-cost catalyst for steam reforming of liquid hydrocarbons.

Acknowledgement

References

[1] S. Martin, G. Kraaij, T. Ascher, P. Baltzopoulou, G. Karagiannakis, D. Wails, A. Worner, Int. J. Hydrogen Energy 40 (2015) 75–84.
[2] C. Song, Catal. Today 77 (2002) 17–49.
[3] I.E. Achouri, N. Abatzoglou, C. Fauteux-Lefebvre, N. Braidy, Catal. Today 207 (2013) 13–20.
[4] N.T.J. Luchters, J.V. Fletcher, S.J. Roberts, J.C.Q. Fletcher, BCREC 2 (1) (2017) 106–112.
[5] G. Dolanc, B. Pregelj, J. Petrovčič, J. Pasel, G. Kolb, J. Power Sources 313 (2016) 223–232.
[6] R.R. Kondakindi, A. Kundu, K. Karan, B.A. Peppley, A. Qi, C. Thurgood, P. Schurer, Appl. Ctalal. A 390 (2010) 271–280.
[7] S. Haji, Y. Zhang, C. Erkey, Appl. Catal. A 374 (2010) 1–10.
[8] S.K. Goud, W.A. Whittenberger, S. Chattopadhyay, M.A. Abraham, Int. J. Hydrogen Energy 32 (2007) 2868–2874.
[9] M. Maestri, D.G. Vlachos, A. Beretta, G. Groppi, E. Tronconi, J. Catal. 259 (2) (2008) 211–222.
[10] C. Fateuteux-Lefebvre, N. Abatzoglou, N. Braidy, I.E. Achouri, J. Power Sources 196 (2011) 7673–7680.
[11] T. Borowiecki, G. Giecko, M. Panczyk, Appl. Catal. A 230 (2002) 85–97.
[12] S.Y. Jung, D.G. Ju, E.J. Lim, S.C. Lee, B.W. Hwang, J.C. Kim, Int. J. Hydrogen Energy 40 (2015) 13412–13422.
[13] A. Vita, C. Italiano, C. Fabiano, L. Pino, M. Laganà, V. Recupero, Appl. Catal. B 199 (2016) 350–360.
[14] C. Xie, Y. Chen, M.H. Engelhard, C. Song, ACS Catal. 2 (2012) 1127–1137.
[15] S.L. Lakhapatri, M.A. Abraham, Appl. Catal. A 364 (2009) 113–121.
[16] Y. Lu, J. Chen, Y. Liu, Q. Xue, M. He, J. Catal. 254 (2008) 39–48.
[17] U. Izquierdo, V.L. Barrio, K. Bizkarra, A.M. Gutierrez, L. Gartzia, J. Bañuelos, I. Lopez-Arbeloa, j.F. Cambra, Chem. Eng. J. 238 (2014) 178–188.
[18] Y.C. Sharma, A. Kumar, R. Prasad, S.N. Upadhyay, Renew. Sust. Energy Rev. 74 (2017) 89–103.
[19] J. Xing, J.F. Chen, Y.H. Li, W.T. Yuan, Y. Zhou, L.R. Zheng, H.F. Wang, P. Hu, Y. Wang, H.J. Zhao, Y. Wang, H.G. Yang, Chem. Eur. J. 20 (2014) 2138–2144.
[20] A. Vita, C. Italiano, C. Fabiano, M. Laganà, L. Pino, Mater. Chem. Phys. 163 (2015) 337–347.
[21] T. Takeguchi, S. Manabe, R. Kikuchi, K. Eguchi, T. Kanazawa, S. Matsumoto, W. Ueda, Appl. Catal. A 293 (2005) 91–96.
[22] 98/70/CE and 2000/71/CE European Community directives. http://eur-lex.europa.eu/ (Accessed 10.04.17).
[23] A. Varma, A.S. Mukasyan, A.S. Rogachev, K.V. Manukyan, Chem. Rev. 116 (2016) 14493–14586.
[24] A. Gayen, K.R. Priolkar, P.R. Sarode, V. Jayaram, M.S. Hegde, G.N. Subbanna, S. Emura, Chem. Mater. 16 (2004) 2317–2328.
[25] M.S. Hegde, G. Madras, K.C. Patil, Acc. Chem. Res. 42 (2009) 704–712.
[26] L. Pino, A. Vita, F. Cipitì, M. Laganà, V. Recupero, Appl. Catal. B 104 (2011) 64–73.
[27] J. Xiaoyuan, L. Guanglie, Z. Renxian, M. Jianxin, C. Yu, Z. Xiaoming, Appl. Surf. Sci. 173 (2001) 208–220.
[28] L. Pino, A. Vita, M. Cordaro, V. Recupero, M.S. Hegde, Appl. Catal. A 243 (2003) 135–146.
[29] H.-H. Liu, Y. Wang, A.-P. Jia, S.-Y. Wang, M.-F. Luo, J.-Q. Lu, Appl. Surf. Sci. 314 (2014) 725–734.
[30] P. Djinović, I.G.O. Črnivec, J. Batista, J. Levec, A. Pintar, Chem. Eng. Process. 50 (2011) 1054–1062.
[31] H.Y. Wang, E. Ruckenstein, Appl. Catal. A 204 (2000) 143–152.
[32] W. Cai, F. Wang, A.C. Van Veen, H. Provendier, C. Mirodatos, W. Shen, Catal. Today 138 (2008) 152–156.
[33] C.-J. Pan, M.-C. Tsai, W.-N. Su, J. Rick, N.G. Akalework, A.K. Agegnehu, S.-Y. Cheng, B.-J. Hwang, J. Taiwan Inst. Chem. Eng. 74 (2017) 154–186, http://dx.doi.org/10.1016/j.jtice.2017.02.012.
[34] C.K.S. Choong, L. Chen, Y. Du, M. Schreyer, S.W.D. Ong, C.K. Poh, L. Hong, A. Borgna, Phys. Chem. Chem. Phys. 19 (2017) 4199–4207.
[35] T. Hou, B. Yu, S. Zhang, T. Xu, D. Wang, W. Cai, Catal. Commun. 58 (2015) 137–140.
[36] C. Italiano, R. Balzarotti, A. Vita, S. Latorrata, C. Fabiano, L. Pino, C. Cristiani, Catal. Today 273 (2016) 3–11.
[37] A.A. Voskanyan, K.-Y. Chan, C.-Y, V. Li, Chem. Mater. 28 (2016) 2768–2775.
[38] X. Xu, P. Li, Y. Shen, Appl. Energy 108 (2013) 202–217.
[39] T.-J. Park, S. Banerjee, T. Hemraj-Benny, S.S. Wong, J. Mater. Chem. 16 (2006) 141–154.
[40] C. Cristiani, E. Finocchio, S. Latorrata, C.G. Visconti, E. Bianchi, E. Tronconi, G. Groppi, P. Pollesel, Catal. Today 197 (2012) 256–264.
[41] G. Cavusoglu, D. Miao, H. Lichtenberg, H.W.P. Carvalho, H. Xuc, A. Goldbach, J.-D. Grunwaldt, Appl. Catal. A 504 (2015) 381–390.
[42] R. Horn, K.A. Williams, N.J. Degenstein, A. Bitsch-Larsen, D. Dalle Nogare, S.A. Tupy, L.D. Schmidt, J. Catal. 249 (2007) 380–393.
[43] A. Simson, R. Farrauto, M. Castaldi, Appl. Catal. B 106 (2011) 295–303.
[44] H.-S. Roh, A. Platon, Y. Wang, D.L. King, Catal. Lett. 110 (2006) 1–6.
[45] B. Cifuentes, M.F. Valero, J.A. Conesa, M. Cobo, Catalysts 5 (2015) 1872–1896.
[46] A.M. da Silva, K.R. de Souza, G. Jacobs, U.M. Graham, B.H. Davis, L.V. Mattos, F.B. Noronha, Appl. Catal. B 102 (2011) 94–109.
[47] J. Pasel, S. Wohlrab, S. Kreft, M. Rotov, K. Löhken, R. Peters, D. Stolten, J. Power Sources 325 (2016) 51–63.
[48] A. Trovarelli, Catal. Rev. Sci. Eng. 38 (1996) 439–520.
[49] A. Tanksale, J.N. Beltramini, J.A. Dumesic, G.Q. Lu, J. Catal. 258 (2008) 366–377.
[50] A. Shamsi, J.P. Baltrus, J.J. Spivey, Appl. Catal. A 293 (2005) 145–152.
[51] G. Mancino, S. Cimino, L. Lisi, Catal. Today 277 (2016) 126–132.
[52] V.S. Guggilla, J. Akyurtlu, A. Akyurtlu, I. Blankson, Ind. Eng. Chem. Res. 49 (2010) 8164–8173.
[53] X. Chen, A.R. Tadd, J.W. Schwank, J. Catal. 251 (2007) 374–387.
[54] X. Chen, B.D. Gould, J.W. Schwank, Appl. Catal A 356 (2009) 137–147.
[55] R.E. Reitmeier, K. Atwood, H. Bennett, H. Baugh, Ind. Eng. Chem. 40 (1948) 620–626.
[56] F. Joensen, J.R. Rostrup-Nielsen, J. Power Sources 105 (2002) 195–201.
[57] Y. Zhang, W. Wang, Z. Wang, X. Zhou, Z. Wang, C.-J. Liu, Catal. Today 256 (2015) 130–136.
[58] F. Frusteri, G. Italiano, C. Espro, C. Cannilla, G. Bonura, Int. J. Hydrogen Energy 37 (2012) 16367–16374.
[59] J.R. Rostrup–Nielsen, Catalytic steam reforming, in: J.R. Anderson, M. Boudart (Eds.), Catal. Sci. Technol., Vol.5, Springer–Verlag, Berlin, 1984.
[60] B.D. Gould, X. Chen, J.W. Schwank, Appl. Catal. A 334 (2008) 277–290.
[61] A.E. Lutz, R.W. Bradshaw, J.O. Keller, D.E. Witmer, Int. J. Hydrogen Energy 28 (2003) 159–167.
[62] M. Ferrandon, J. Mawdsley, T. Krause, Appl. Catal. A 342 (2008) 69–77.
[63] J. Koningen, K. Sjöström, Ind. Eng. Chem. Res. 37 (1998) 341–346.
[64] S. Morita, T. Inoue, Int. Chem. Eng. 5 (1965) 180–185.
[65] S. Appari, V.M. Janardhanan, R. Bauri, S. Jayanti, Int. J. Hydrogen Energy 39 (2014) 297–304.
[66] C. Xie, Y. Chen, Y. Li, X. Wang, C. Song, Appl. Catal. A 394 (2011) 32–40.
[67] Y. Chen, C. Xie, Y. Li, C. Song, T.B. Bolin, Phys. Chem. Chem. Phys. 12 (2010) 5707–5711.
[68] P.K. Cheekatamarla, W.J. Thomson, J. Power Sources 158 (2006) 477–484.
[69] S. Ahmed, R. Kumar, M. Krumpelt, Fuel Cells Bull. 2 (1999) 4–7.
[70] G. Garbarino, A. Lagazzo, P. Riani, G. Busca, Appl. Catal. B 129 (2013) 460–472.
[71] Q. Zheng, C. Janke, R. Farrauto, Appl. Catal. B 160–161 (2014) 525–533.
[72] A.M. Azad, D. Sundararajan,Adv Mater. Sci. Eng. (2010), 681574 15, Colume 2010.
[73] J. Park, J. Noh, J. Chang, S. Park, Catal. Lett. 65 (2000) 75–78.
[74] N. Laosiripojana, S. Charojrochkul, P. Kim-Lohsoontorn, S. Assabumrungrat, J. Catal. 276 (2010) 6–15.
[75] P.K. Cheekatamarla, A.M. Lane, J. Power Sources 152 (2005) 256–263.
[76] R.M. Ferrizz, R.J. Gorte, J.M. Vohs, Appl. Catal. B 43 (2003) 273–280.